#25-089
2025 AFS Proceedings ©American Foundry Society

Understanding the Effects of Boron on the Microstructure and Mechanical Properties of Pearlitic Ductile Irons

Colleen P. Lehrer
Laura N. Bartlett, Simon N. Lekakh
Missouri University of Science and Technology, Rolla, Missouri, USA

Copyright 2025 American Foundry Society

ABSTRACT

Boron is noted to effectuate change on the microstructure and mechanical properties of spheroidal graphite irons (SGI). A pearlitic grade of SGI with 0.9 wt.% Cu and 0.4 wt.% Mn was investigated for sensitivity to boron contamination. In a laboratory melted SGI, boron additions were controlled from 12 to 95 ppm. The SGI was cast into step blocks containing section thicknesses from 5- to 50-mm and an integrated thermal analysis cup. Additions up to 39 ppm B decreased the temperature at the end of solidification and raised the eutectoid temperatures of interest. Quantitative analysis of microstructure was performed, and it was shown that effects of boron contamination varied with cooling rate. More prominent negative effects on graphite morphology and increased ferrite content were detected in thin sections. Boron additions up to 39 ppm were observed to decrease the tensile and yield strengths of the pearlitic SGI.

Keywords: spheroidal graphite iron, SGI, boron, solidification, microstructure, mechanical properties

INTRODUCTION

As cast iron with spherical graphite (SGI) is very pure during melt treatment, this material can be significantly more sensitive to trace element contamination when compared to other ferrous- or aluminum-based cast alloys. For example, the deleterious effect of Fe contamination on aluminum alloys takes place above the thousands of ppm range, while sulfur and oxygen on the order of hundreds of ppm destroy the nodular graphite shape in SGI. Moreover, some elements at only the tens of ppm level affect the structure and properties of SGI. One such impurity which cannot be effectively removed from the melt by currently known purification technology is boron.

There are several intrinsic sources of B contamination in SGI, such as the micro-alloying of steels with boron which has become increasingly attractive within the automotive industry and gives rise to contamination of foundry scrap supply. Boron contamination may also be added to the melt from extrinsic sources, such as from induction furnace linings. Due to cost restrictions associated with using a high purity charge to dilute the melt, it is important to quantify the effect of boron and determine a feasible contamination window for different types of SGI and range of casting wall thicknesses.

Quantification of the effects of boron may be difficult due to the possibility of chemical reactions of B with other melt contaminants, such as nitrogen, as well as competing reactions to form nitrides with more active elements (Ti and Zr). Pawaskar et al.[1] performed thermodynamic simulations of competing reactions in the iron melt and during cooling of cast iron. The mutual effects of B, N, and Ti micro-additions were determined, and a “free B” concept was suggested to link ferrite promotion in B-contaminated cast iron. This hypothesis was simulated for different B additions as well as to predict the mutual effect of other impurities in cast iron. The thermodynamic simulations showed that elevated N can be used to tie down B and avoid B interactions with the metal matrix during the eutectoid reaction. On the other hand, a common impurity such as Ti could compete for N and increase the “free B,” thereby promoting ferrite formation. It is important to note that suggested methodology will be used by the authors of this article for quantitative predictions of critical concentrations of multiple impurities in SGI in presence of free Mg.

Experimental determination of the effects of B contamination on SGI structure has been done over the last decades. An overview of recent studies,[2-4] including reviews of previous studies is provided: Bugten et al.[2] studied effects of boron at concentrations ranging from 5 to 525 ppm in low-Cu SGI and no effect was observed on the size distribution, graphite number density, or shape morphology. However, B was observed to lead to a rough surface morphology of the graphite nodules at concentrations above 24 ppm and intercellular carbides were found in SGI with more than 70 ppm B.

Ha et al.[3] also examined the mutual effect of B contamination and copper, a common pearlite stabilizer. Boron increased the ferrite content whereas copper augmented the stability of pearlite and the interaction between these elements significantly influences the ferrite

content. Mechanical property assessments showed that B decreases the tensile and yield strengths of SGI but simultaneously enhances elongation. It was suggested that B microalloying could help utilization of copper-bearing scrap for ferritic nodular cast iron.

Effect of 10, 49 and 131 ppm B contamination on the microstructure and mechanical properties of GJS-500-7 grade SGI at different wall thicknesses was studied by Kasvayee et al.[4] Addition of 49 ppm boron decreased pearlite fraction by nearly 1/3 in all cast plates. Variation in the plate thickness did not affect the pearlite fraction and minor changes were observed in the pearlite fraction by increasing B from 49 to 131 ppm. Recent work[5] investigated the synergetic effect of 44 ppm B with additions of Sn, Cu and Mn.

The results show that up to 0.9 wt.% Mn is not enough to promote a fully pearlitic matrix, while 0.5 wt.% Cu or 0.06 wt.% Sn combined with 0.67 wt.% Mn is sufficient. In all studied cases, B was found to promote ferrite in fully pearlitic SGI alloyed with Sn or Cu; however, in the absence of those elements, B promoted pearlite. Graphite protrusions were observed on the graphite nodule surface only for B-added alloys with Sn and Cu. The authors suggested that B promotes ferrite by changing the growth mechanism of graphite after solidification from spherical to lamellar.

From these publications, it could be concluded that a straightforward B effect was not observed due to the mutual influence of other factors, including SGI chemistry and cooling rate. Therefore, the goal of this project was determination of synergetic effects of B in SGI. This paper contains the results of the first part of this study.

DESIGN OF EXPERIMENTS

Several identical procedure heats were performed in a 200-lb induction furnace using an industrial grade charge of known composition. The B level was controlled by FeB additions into the melt. Two heats with variations in residual B at approximately the same concentrations of the other elements will be discussed in this article. To stabilize chemistry and ladle treatment, melting was conducted under constant-flow argon gas and an insulating ceramic blanket. Alloying with manganese and copper was used to promote pearlite. At 1530C (2786F), the melt was tapped into a preheated ladle containing 0.3% of the total melt weight of inoculant and sufficient nodulizer to target 350ppm Mg, with recovery considered. The inoculant was a 75% FeSi-based inoculant with Al and Ba additions, and the nodulizer contained 4% Mg and rare-earth metals. After pouring each chemistry, a serial in-ladle plunge addition of a FeB alloy was used to increase the boron content. Four alloys were produced with boron levels of 12, 27, 39, and 95 ppm respectively (Table 1).

Each SGI was cast into a specially designed mold made from silica sand with phenolic nobake binder. The mold included a step block (5, 15, 30, and 50-mm section thicknesses) combined with a chill wedge, copper-chilled specimen for chemical analysis, and one K-type thermal analysis cup (Fig. 1). Each casting was top-risered with an insulating sleeve located above the centroid of the 50 mm step. Vents (¼ inch diameter) were located above each casting, and the end of the step block had additional overflow volume. For the evaluation of mechanical properties, each SGI was also cast into two ASTM A536 modified keel blocks which were machined to create four ASTM A536 1¾ in. reduced section (1.4” gage length with 0.357” diameter) tensile bars.

Samples for optical microscopy (OM) were sectioned from six locations: the centroid of each step, center of the thermal analysis cup, and offcut sections of representative tensile bars. Brinell hardness (HBW 10/3000) was obtained at the longitudinal centerline of each step block section and within tensile bar offcuts. Final alloy composition was established using optical emission spectroscopy (OES) of white-solidified samples and combustion analysis of the centroid of the largest casting section.

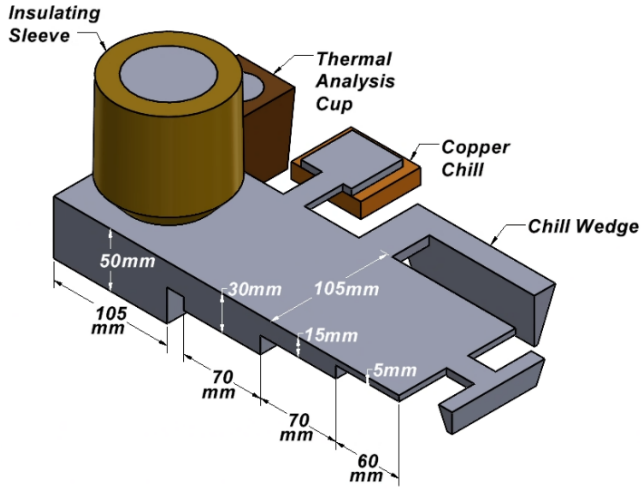

Figure 1. Schematic of castings produced in combined mold.

Table 1. Target Chemical Compositions of Studied SGI

Chem.	CE (wt.%)	C (wt.%)	Si (wt.%)	Mn (wt.%)	Mg (ppm)	Cu (wt.%)	Sn (wt.%)	B (ppm)
A	4.22	3.49	2.46	0.48	280	0.95	0.006	12±1
B	4.26	3.46	2.57	0.42	280	0.91	0.007	27±2
C	4.29	3.46	2.69	0.42	270	0.91	0.007	39±2
D	4.28	3.46	2.64	0.42	240	0.92	0.007	95±4

RESULTS & DISCUSSION

Thermal analysis provides important information about liquid-solid and solid-solid transformations by tracking latent heat liberation. In this study, incorporation of thermal analysis cups into the molds ensured similar pouring conditions for each cup and its respective casting. Postprocessing of collected cooling curves included determination of critical points by tracking first and second derivative. Figure 2 presents solidification and Fig. 3 illustrates austenite decomposition during eutectoid reaction. In addition, the first derivative vs. temperature was used to clarify eutectoid reaction. Extracted parameters are presented in Table 2. For solidification, the temperatures of eutectic minimum (T_{Emin}), eutectic maximum (T_{Emax}), and at the end of solidification (T_{sol}) were calculated using first and second derivatives. For eutectoid reaction, eutectoid maximum was determined directly from the cooling curve, and the velocity of transformation (V_{Trans}) and its corresponding temperature (T_{Trans}) were determined from the maximum of the first derivative with respect to time, after the application of a moving average of five data points. Solidification data for 27ppm B was not recorded due to an equipment malfunction.

In quantities up to 39 ppm, B addition was found to increase T_{Emin} and T_{Emax}, as well as decrease T_{sol}. However, beyond 39 ppm, additional B had little effect on T_{Emin} and T_{Emax}. These results could be interpreted as medium B contamination (up to 39 ppm) stimulated nucleation; however, segregation in last solidified regions suppressed later graphite growth which may promote carbide formation at fast cooling rates. However, a corresponding increase in graphite number density with boron content was not observed to a statistically significant confidence (Fig. 5c). The B contamination was found to have a strong effect on the eutectoid rection. It is necessary to note that the latent heat of the eutectoid reaction is an order of magnitude less than that of solidification and has a smaller impact on the cooling curve; however, thermal analysis indicated a significant B effect (Fig. 3). Increasing boron content up to 39 ppm resulted in increased temperatures of eutectoid minimum, maximum, and T_{Trans}. Together with a significant decrease in the transformation velocity, V_{Trans}, these changes indicated ferrite promotion under such B addition. Further increase in B contamination stabilized, but did not accelerate, the ferrite forming effect.

Predictions from thermal analysis of boron's effect on solidification structure and the metal matrix during the eutectoid reaction were verified with quantitative metallography. In this case, the structure was analyzed in different sections of the step plates to quantify combined effects of B contamination and cooling rate.

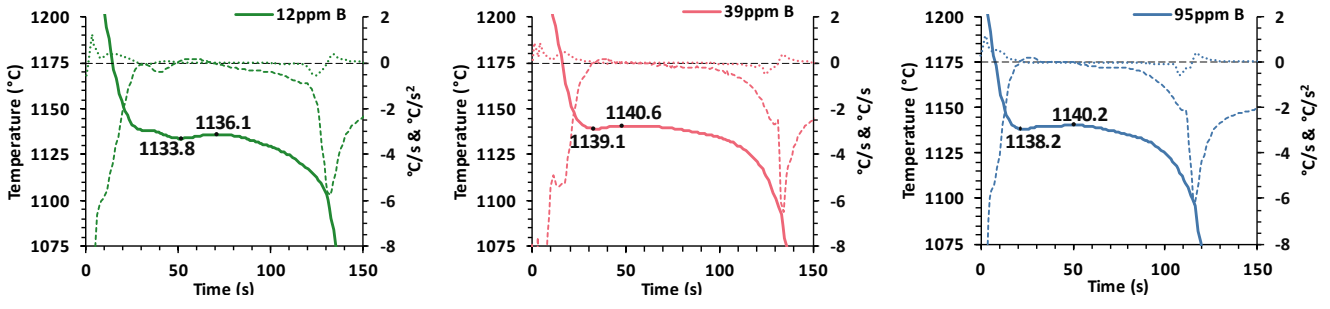

Figure 2. Thermal analysis of solidification in SGI with 12, 39, and 95 ppm B (solid lines – cooling curves, dashed lines – first derivative, and dotted lines – second derivative).

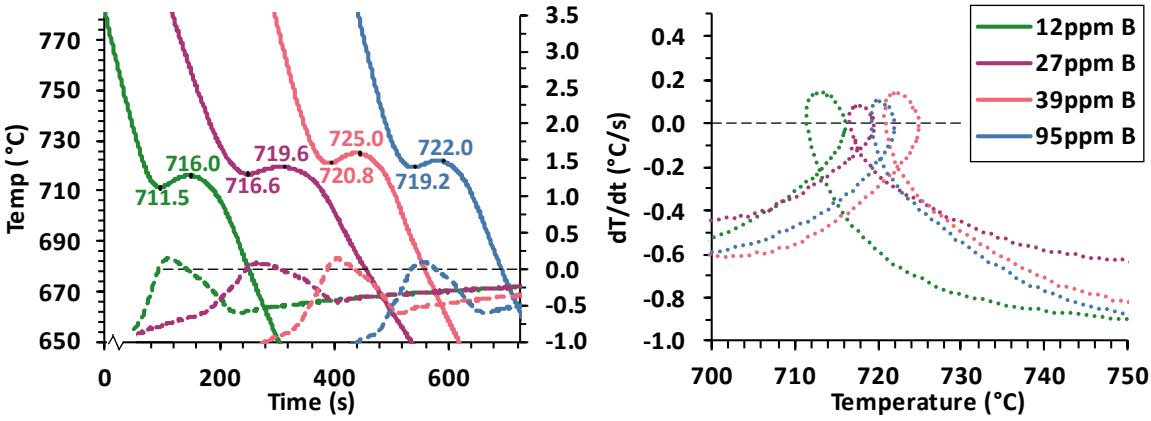

Figure 3. Thermal analysis of eutectoid in SGI with different levels of B contamination: (a) cooling curves (solid lines) and first derivative (dotted lines) and (b) first derivative vs temperature. Time shifted arbitrarily for clarity.

Table 2. Quantitative Analysis of Cooling Curves for Eutectic and Eutectoid Reactions in SGI

	12 ppm *B*	27 ppm *B*	39 ppm *B*	95 ppm *B*
Solidification				
Eutectic Minimum, T_{Emin} (C)	1133.8	-	1139.1	1138.2
Eutectic Maximum, T_{Emin} (C)	1136.1	-	1140.6	1140.2
Solidus, T_{Sol} (C)	1108.1	-	1104.1	1106.0
Eutectic Recalescence, ΔT (°C)	2.3	-	1.5	2.0
Eutectoid				
Eutectoid Min (C)	711.5	716.6	720.8	719.2
Eutectoid Max (C)	716.0	719.6	725.0	722.0
Eutectoid Recalescence, ΔT (°C)	4.6	3.0	4.2	2.8
T_{Trans} (C)	713.2	717.7	722.7	720.3
V_{Trans} (C/s)	0.148	0.085	0.146	0.107

Representative micrographs from the centroids of step block sections, tensile bars, and thermal analysis cups are shown in Fig. 4. Corresponding descriptors of microstructure quality are shown in Fig. 5 for the graphite phase and Fig. 6 for the metal matrix.

Using as-polished specimens, the graphite phase was classified as particulate with an area greater than 10 μm^2 on optical micrograph. Nodularity was assessed by count, using the roundness shape factor (RSF) from ISO 945-4: the quotient of the measured area of each particle and a circle of its maximum Feret diameter. Any particulate with RSF > 0.60 was considered nodular. Variations in measured nodularity did not allow a statistically significant conclusion with respect to boron content.

These specimens were used for an additional study: a new method for determination of graphite shape using a chord algorithm via automated scanning electron spectroscopy with energy dispersive X-ray spectroscopy and preliminary results are available.[6]

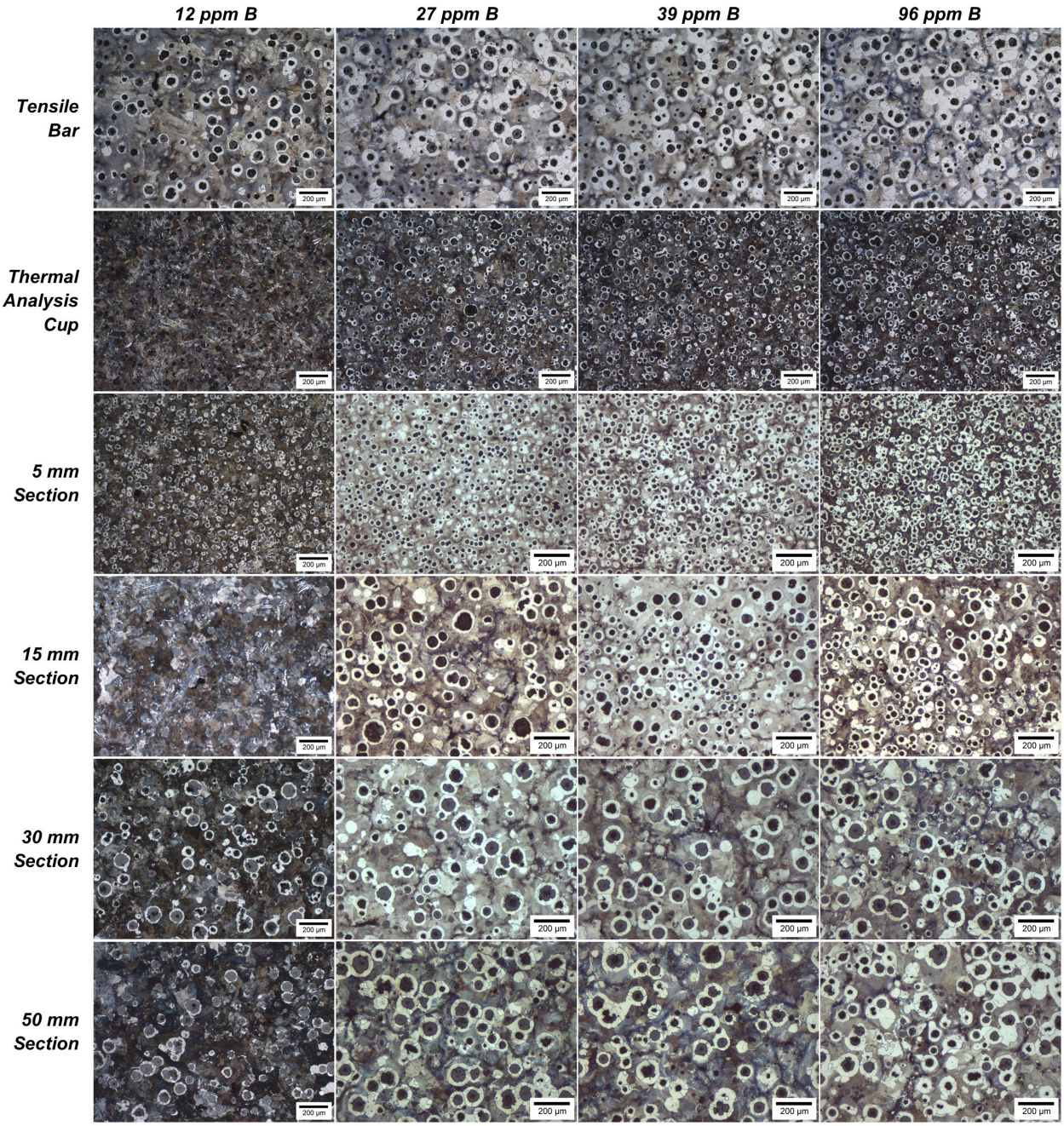

Figure 4. Etched microstructures in studied SGI at different locations.

Optical imaging analysis of the metal matrix (i.e., ferrite and pearlite fraction) is based on measured area via pixel number to quantify microstructure (Fig. 6). For the step blocks, ferrite fraction increased with boron content for all section thicknesses for additions up to 39 ppm B, albeit the ferrite fraction did not show a statistically significant increase above 39 ppm B.

Only in the fast-cooled 5-mm steps did ferrite content continue to increase with increasing B contamination. These results correlated well with the effects of boron predicted by thermal analysis of the solidification and eutectoid transformations.

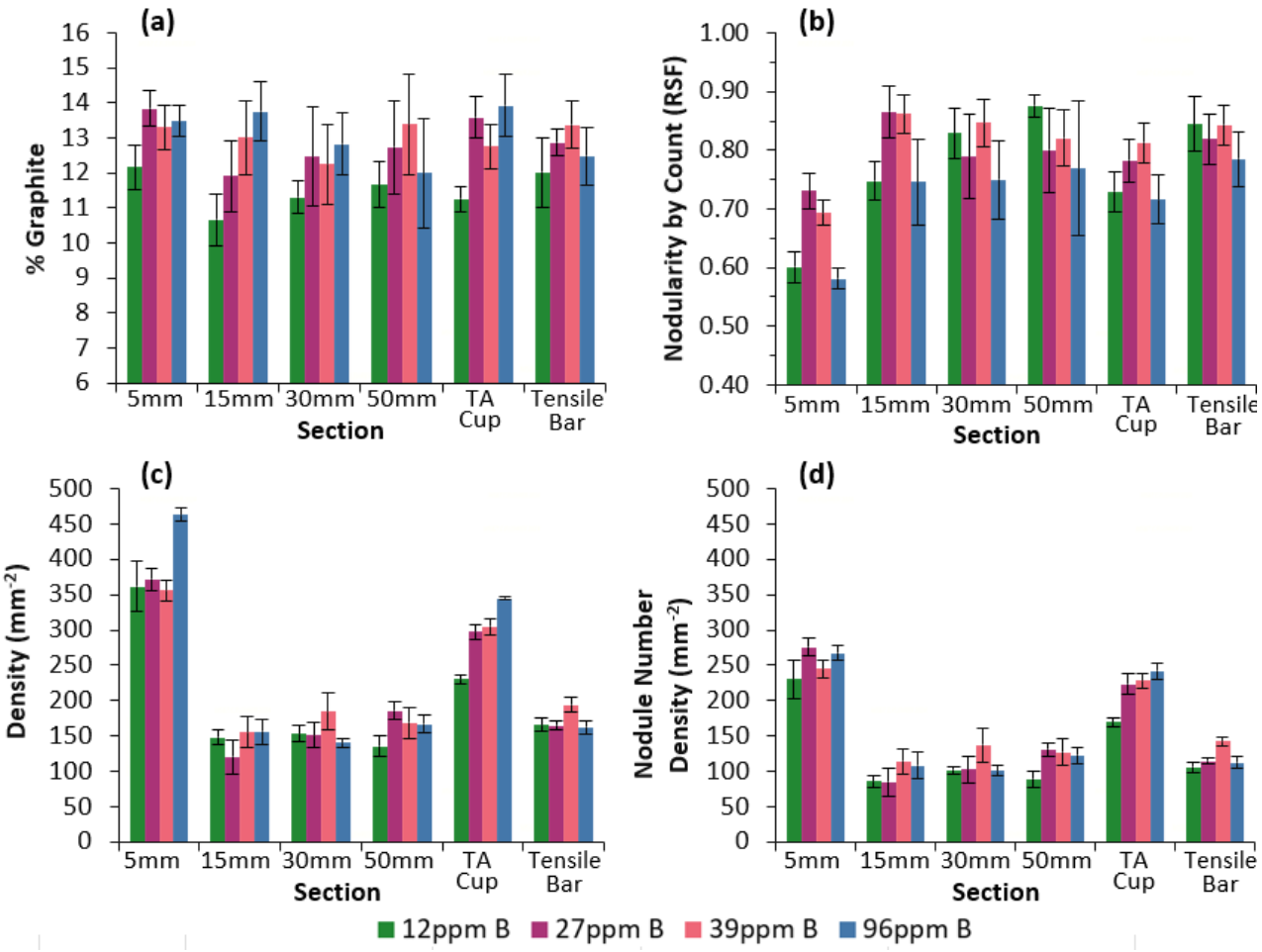

Figure 5. Quantitative analysis of the graphite phase.

In Figure 7a, data is summarized for Brinell hardness taken at the centerline of the tensile bars and centerline of the 15-, 30-, and 50-mm section thickness steps. A decrease in hardness with boron addition was significant for all cooling rates, with fast-cooled SGI showing higher sensitivity to B contamination. Representative examples of tensile results are shown in Figure 7b. Ultimate tensile strength and 0.2% offset yield strength were observed to have a sharp, and then steady decline, up to and after 27 ppm B, respectively (Table 3). The greatest elongation at fracture was observed at moderate (27 and 39 ppm) boron levels, while the low and high (12 and 96 ppm) boron samples had lower elongation at fracture. These results correlated well with observed changes in microstructure.

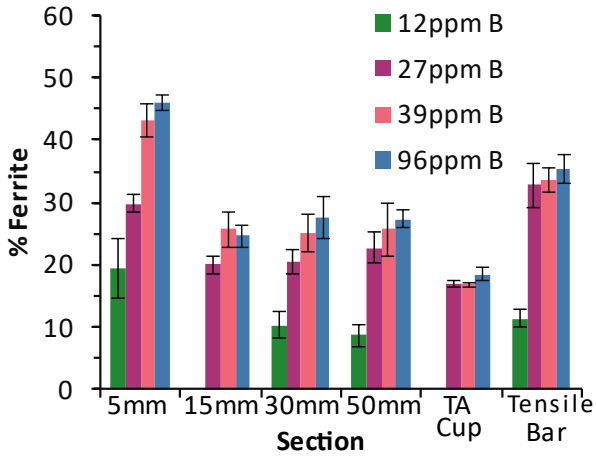

Figure 6. Quantitative analysis of the metal matrix.

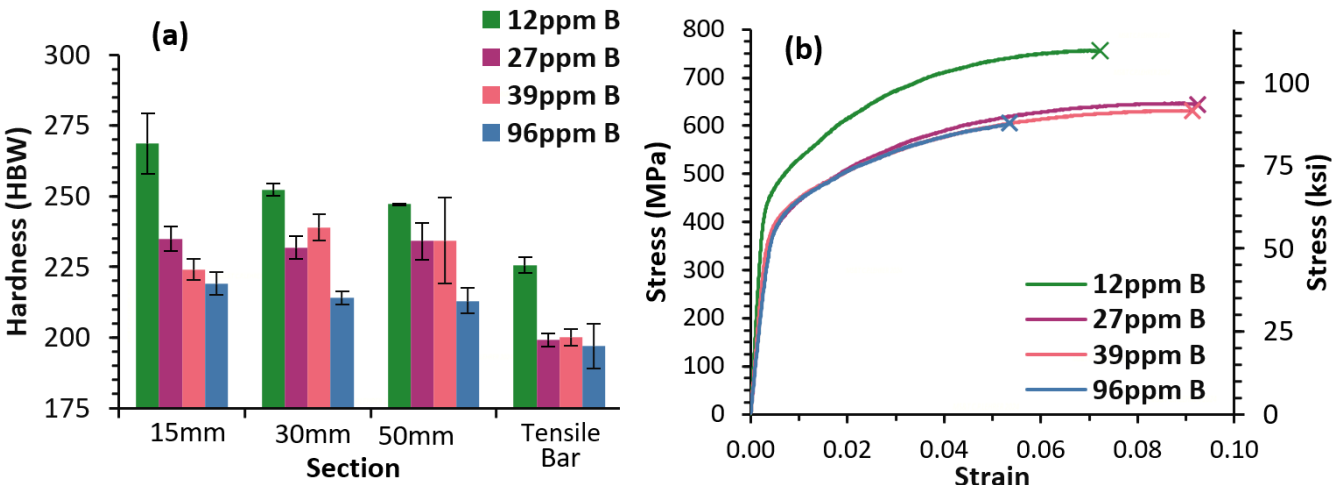

Figure 7. Effect of boron contamination on mechanical properties: (a) hardness and (b) tensile strength.

Table 3. Effect of Boron Contamination on Tensile Properties of SGI

Boron, ppm	12	27	39	96
Ultimate Tensile Strength, MPa	732±28	643±25	633±11	612±21
0.2 Yield Strength, MPa	461±19	396±13	406±7	407±10
Elongation, %	6.6±1.1	9.4±0.3	8.6±1.0	5.9±0.8

CONCLUSION

A set of laboratory heats of pearlitic SGI with tight control of B contamination were conducted, producing specially designed castings with step plates and incorporated thermal analysis cups. Thermal analysis and quantification of structural features were used to determine the effect of contamination B at different cooling rates. It was shown that up to 39 ppm, boron contamination promoted ferrite formation, and this effect is more prominent at higher cooling rates. These results will be used in an ongoing study to develop a novel model for SGI where mutual effects of chemistry, degree of contamination by minor elements, and casting cooling rate will be quantified to predict properties and optimize melting practice.

ACKNOWLEDGMENTS

This AFS Research Project, 22-23#06, “Understanding and Mitigating the Effect of Boron in Ductile Iron,” is an active research project that is monitored by the Cast Iron Research Committee under the Cast Iron Division.

REFERENCES

1. Pawaskar, S., Bartlett, L., Lekakh, S., Mutual B, Ti, N effects on phase transformations in cast iron: Thermodynamic consideration and experimental verification. *AFS Trans.* **130**, 185-195 (2022).
2. Bugten, A.V., Michels, L., Brurok, R.B., et al., “The Role of Boron in Low Copper Spheroidal Graphite Irons,” *Metall Mater Trans A* 54, 2539–2553 (2023). https://doi.org/10.1007/s11661-023-07014-y (Link last accessed 03-31-25.)
3. Ha, J., Hong, J., Kim, J., et al., “The Effect of Boron (B) and Copper (Cu) on the Microstructure and Graphite Morphology of Spheroidal Graphite Cast Iron,” *Materials* 2023, 16(12), 4225; https://doi.org/10.3390/ma16124225 (Link last accessed 02-19-25.)
4. Kasvayee, K., Ciavatta, M., Ghassemali, E., et al., “Effect of Boron and Cross-Section Thickness on Microstructure and Mechanical Properties of Ductile Iron,” *Materials Science Forum*, 925 (2018) 249-256. https://doi.org/10.4028/www.scientific.net/msf.925.249 (Link last accessed 02-19-25.)
5. Bugten, A.V., Sanders, P., Hartung, C. *et al.* The Influence of Boron (B), Tin (Sn), Copper (Cu), and Manganese (Mn) on the Microstructure of Spheroidal Graphite Irons. *Inter Metalcast* **18**, 1914–1925 (2024). https://doi.org/10.1007/s40962-023-01218-z (Link last accessed 03-31-25.)
6. Schroeder, C., Lehrer, C., Lekakh, S., Bartlett, L., “A Novel Technique for Improved Measurement of Graphite and Inclusions in Ductile Iron Contaminated by Boron,” *AFS Metalcasting Congress Proceedings*, #25-079 (2025).